

NASA Technical Paper 3547

# Method for the Calculation of Spacecraft Umbra and Penumbra Shadow Terminator Points

Carlos R. Ortiz Longo and Steven L. Rickman  
*Lyndon B. Johnson Space Center*  
*Houston, Texas*

April 1995

This publication is available from the NASA Center for Aerospace Information, 800 Elkridge Landing Road, Linthicum Heights, MD 21090-2934 (301) 621-0390.

# Contents

Section	Page
List of Symbols.....	v
Abstract.....	1
Introduction.....	1
Shadow Analysis Methodology.....	2
Definition of Shadow Cone Surfaces.....	2
Definition of Umbra and Penumbra Terminator Parameters.....	4
Determination of the Spacecraft Location.....	8
Quaternions.....	8
Quaternion Algebra.....	9
Vector Transformations.....	12
Motion in the Orbit Plane.....	12
Calculation of the $\vec{r}_{M50}$ Vector.....	13
Iterative Methodology.....	16
Sample Cases.....	17
High Inclination, Low-Earth Orbit.....	18
Sun-Synchronous Orbit.....	20
High Inclination Elliptical Orbit.....	22
Geostationary Orbit.....	24
CRRES Orbit.....	26
Conical versus Cylindrical Assumption.....	28
References.....	29

## Tables

	Page
1 Orbital Parameters of Sample Case 1 .....	19
2 Orbital Parameters of Sample Case 2 .....	21
3 Orbital Parameters of Sample Case 3 .....	23
4 Orbital Parameters of Sample Case 4 .....	24
5 Orbital Parameters of Sample Case 5 .....	26
6 Orbital Parameters of Sample Case 6 .....	28
7 Comparison of Conical and Cylindrical Shadow Assumptions.....	28

## Figures

1 Schematic representation of a planet's shadow regions.....	2
2 Representation of the umbral cone geometry.....	3
3 Representation of the penumbral cone geometry.....	4
4 Representation of the $\bar{r}_s$ and $\bar{\delta}$ vectors.....	5
5 Location of the penumbral cone terminator at the projected spacecraft location.....	6
6 Location of the umbral cone terminator at the projected spacecraft location.....	6
7 Polar coordinate definition of in-plane orbit parameters.....	13
8 Definition of spacecraft location in the M50 reference frame.....	14
9 Case 1: Beta angle variation with time.....	19
10 Case 1: Percent time in shadow.....	20
11 Case 2: Beta angle variation versus time.....	21
12 Case 2: Percent time in shadow.....	22
13 Case 3: Beta angle variation versus time.....	23
14 Case 3: Percent time in shadow.....	24
15 Case 4: Beta angle variation versus time.....	25
16 Case 4: Percent time in shadow.....	25
17 Case 5: Beta angle variation versus time.....	27
18 Case 5: Percent time in shadow.....	27

## List of Symbols

$\alpha_p$	penumbral subtended angle
$\alpha_u$	umbral subtended angle
$\beta$	angle between solar vector and its projection onto the orbit plane
$\Gamma$	ecliptic solar longitude
$\varepsilon$	obliquity of the ecliptic
$\chi_p$	distance between the penumbral cone apex and the center of the planet
$\chi_u$	distance between the umbral cone apex and the center of the planet
$\delta_{p-s}$	planet to sun distance
$\bar{\delta}$	vector originating at the umbral cone axis, pointing to the spacecraft at projected spacecraft location
$\phi$	principal angle
$\kappa$	distance between the umbral cone axis and the penumbra terminator point, at the projected spacecraft location
$\mu$	planet gravitational parameter
$v$	true anomaly
$\xi$	distance between the umbral cone axis and the umbra terminator point at the projected spacecraft location
$\omega$	argument of pericenter
$\Delta_p$	penumbra shadow terminator variable
$\Delta_u$	umbra shadow terminator variable
$\Omega$	right ascension of the ascending node
$a$	orbit semimajor axis
$e$	orbit eccentricity
$e_x, e_y, e_z$	components of the principal axis
$i$	orbit inclination
$\hat{i}, \hat{j}, \hat{k}$	orthogonal cartesian unit vectors
$\hat{o}$	orbit normal vector
$p$	parameter or semi-latus rectum
$r_{eq}$	planet/moon equatorial radius
$\bar{r}_{M50}$	vector pointing from the center of the planet to the spacecraft
$\bar{r}_s$	projection of the $\bar{r}_{M50}$ vector onto the unit solar vector
$\hat{r}_\gamma$	Reference Vector (M50)
$\hat{r}_{p \rightarrow sp}$	unit vector pointing from the center of the planet to the spacecraft (M50 ref. frame)
$\hat{s}$	solar unit vector
$D_p$	diameter of the planet
$D_s$	diameter of the sun

E        eccentric anomaly  
J<sub>2</sub>      oblateness perturbation coefficient

## Abstract

A method for calculating orbital shadow terminator points is presented. The current method employs the use of an iterative process which is used for an accurate determination of shadow points. This calculation methodology is required, since orbital perturbation effects can introduce large errors when a spacecraft orbits a planet in a high altitude and/or highly elliptical orbit. To compensate for the required iteration methodology, all reference frame change definitions and calculations are performed with quaternions. Quaternion algebra significantly reduces the computational time required for the accurate determination of shadow terminator points.

## Introduction

In an effort to enhance the analysis capabilities of the Thermal Branch of the Structures and Mechanics Division at the Johnson Space Center, the authors are currently developing an analysis tool that will help in the design of a spacecraft mission attitude timeline based on the definition of thermal and power constraints. An important consideration of this task is the understanding of the duration of shadow passage for any given mission timeline, for this phenomenon has a significant effect on the on-orbit thermal environment experienced by a spacecraft.

The problem of calculating the shadow times of a spacecraft orbiting a body has been studied in depth by various methods.<sup>1-10</sup> Assuming that the celestial bodies are spherical in shape, a planet's shadow consists of two distinct conical projections: the umbra and the penumbra (Figure 1). For the most part, however, the umbral shadow has been treated as a cylindrical projection of the Earth,<sup>1-5</sup> since it significantly simplifies the calculation methodology. This assumption is fairly accurate for low altitude circular orbits but may lead to significant terminator point calculation errors for high altitude or highly elliptical orbits, in addition to ignoring the penumbral effects. Other authors<sup>6-10</sup> have treated the conical shadow projections. Peckman<sup>6</sup> treated only the umbral cone, while the others<sup>7-10</sup> have treated the effects of both shadow regions. However, these analyses have ignored orbit perturbation effects during propagation of the orbit. For thermal environment calculations, solar motion and perturbations give rise to the variation in the  $\beta$  angle, and ignoring these perturbations may lead to incorrect calculation of the environment, especially at  $\beta$  angle extremes where the spacecraft may be experiencing an unclipped orbit. The consideration of perturbation effects is required for an accurate calculation of shadow passage time. Additionally, only Dreher<sup>8</sup> has accounted for the effect of refraction in the shadow passage time.

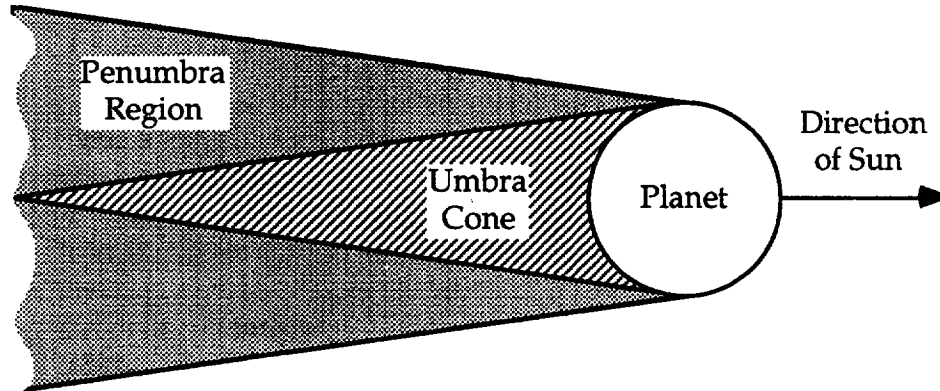


Figure 1. Schematic representation of a planet's shadow regions.

The current method is considered as an enhancement of the Long model.<sup>4</sup> Through the use of an iterative procedure, the shadow passage times are calculated considering conical projections of umbral and penumbral shadows and perturbation effects. The current method does not consider refraction effects.

### Shadow Analysis Methodology

The size and shape of the umbral and penumbral shadow regions are mainly functions of the planet size, the size of the sun, and the distance between the two celestial bodies. The refractive effects of the planet's atmosphere, although not considered in this analysis, could also affect the shadow geometries and therefore passage times.<sup>7,8</sup> The umbra region is characterized by the total blockage of the solar energy component and the penumbra region by the partial blockage of the sun disk by the planet. In this region, the component of solar heating varies between a zero value at the umbra terminator to full solar at the penumbra terminator point.<sup>7</sup>

The calculation of shadow terminator points will be defined from the projection of the spacecraft onto the shadow cones, and the definition of the vector that points from the center of the umbral cone to the spacecraft at the projected site. The location of the spacecraft is calculated in the Mean of 1950 (M50) reference frame. The transformation calculations are performed using quaternion algebra, which significantly accelerates computation time.

#### Definition of Shadow Cone Surfaces

As in all of the shadow analyses considered,<sup>6-10</sup> this method assumes the celestial bodies to be spherical in shape, therefore, producing a conical projection of the shadow regions. (Note: the effects of a nonspherical body are accounted for only in the sense that they perturb the orbit.) This allows for the description of the umbral cone simply by considering the planet and sun diameters and the



separation between them. Then from geometry (Figure 2), we can calculate the umbral geometry from

$$\chi_u = \frac{D_p \delta_{p-s}}{(D_s - D_p)} \quad (1)$$

and

$$\alpha_u = \sin^{-1} \frac{D_p}{2\chi_u}. \quad (2)$$

In the same way, the penumbral cone geometry can be determined (Figure 3) from

$$\chi_p = \frac{D_p \delta_{p-s}}{(D_s + D_p)} \quad (3)$$

and

$$\alpha_p = \sin^{-1} \frac{D_p}{2\chi_p}. \quad (4)$$

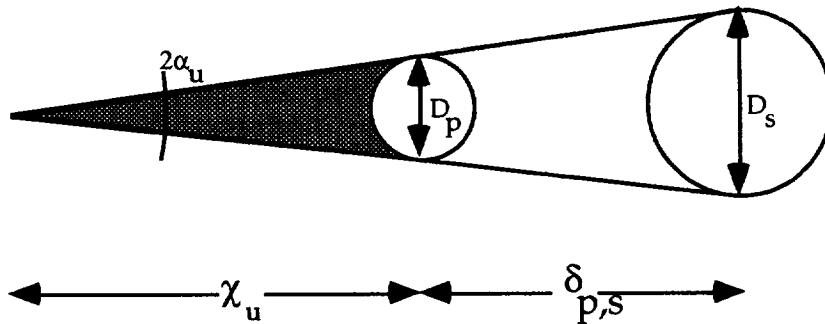


Figure 2. Representation of the umbral cone geometry.

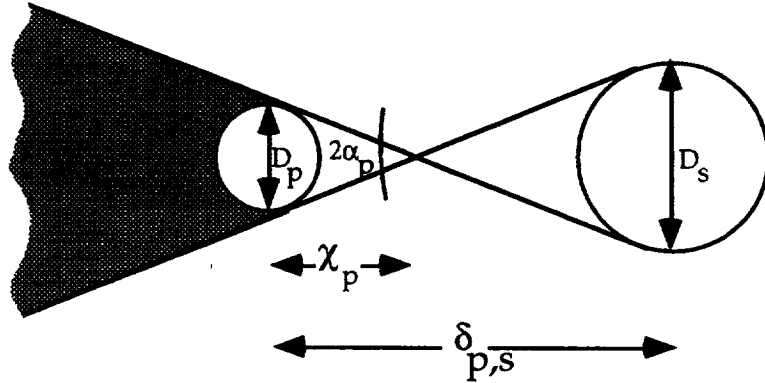


Figure 3. Representation of the penumbral cone geometry.

### Definition of Umbra and Penumbra Terminator Parameters

The definition of the shadow terminator points is accomplished by locating the umbral and penumbral cones terminators at the projected spacecraft location. The location of the spacecraft in the M50 reference frame is represented by the  $\vec{r}_{M50}$  vector and is deferred to a later section. Figure 4 depicts the vector  $\vec{r}_s$  which defines this projection. The projection vector is obtained from the dot product of the vectors  $\vec{r}_{M50}$  and  $\hat{s}$ , that is

$$\vec{r}_s = (\vec{r}_{M50} \cdot \hat{s}) \hat{s}. \quad (5)$$

Note that a shadow terminator may only be found when  $(\vec{r}_{M50} \cdot \hat{s}) < 0$ , as previously recognized by others.<sup>4</sup> With the definition of the  $\vec{r}_s$  vector, a second vector,  $\vec{\delta}$ , can be defined from

$$\vec{\delta} = \vec{r}_{M50} - \vec{r}_s. \quad (6)$$

The  $\vec{\delta}$  vector represents the distance between the center of the umbral cone and the spacecraft, at the projection point. Note that for the simplified assumption of a cylindrical umbral shadow projection, if the magnitude of the  $\vec{\delta}$  vector is less than the radius of the planet, the spacecraft is considered to be in the planet's shadow. In the same way, the shadow terminator is found when the magnitude of the  $\vec{\delta}$  vector is equal to the planet's radius.<sup>4-5</sup> Note that this analysis does not consider the case of a spacecraft orbiting a planet beyond the apex of the umbral cone. This assumption, however, is justified by the small subtended angles

associated with the umbral cone shadow geometry, which locates the umbral cone apex at great distances from the center of the planet.

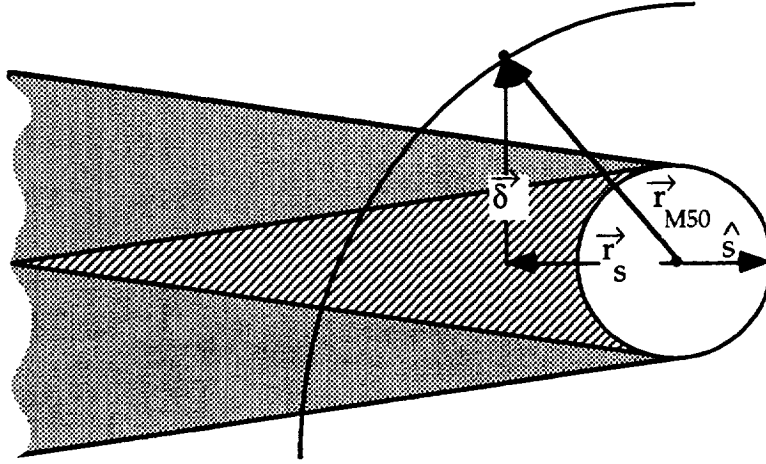


Figure 4. Representation of the  $\bar{r}_s$  and  $\bar{\delta}$  vectors.

In addition to the  $\bar{\delta}$  vector, the determination of the  $\bar{r}_s$  vector allows for the location of the shadow terminator points at the specific projected location. From Figures 5 and 6, the distances  $\kappa$  and  $\xi$  are defined as

$$\xi \equiv (\chi_u - |\bar{r}_s|) \tan \alpha_u \quad (7)$$

and

$$\kappa \equiv (\chi_p + |\bar{r}_s|) \tan \alpha_p. \quad (8)$$

The parameter  $\xi$  represents the distance between the center of the umbral cone and the umbral cone terminator, at the projected spacecraft location. In the same way,  $\kappa$  represents the distance between the center of the umbral cone and the penumbra terminator, at the projected spacecraft location.

As evidenced, a simple comparison between the magnitude of the  $\bar{\delta}$  vector and  $\kappa$  and  $\xi$  defines the shadow terminator points. Specifically, the following comparisons may be drawn:

- a) Shadow terminators may only be encountered when  $(\bar{r}_{M50} \bullet \hat{s}) < 0$ .
- b) However, the spacecraft will still be in sunlight if  $|\bar{\delta}| > \kappa$ .
- c) The spacecraft is in penumbra if  $\xi < |\bar{\delta}| < \kappa$ .

- d) The spacecraft is in umbra if  $|\bar{\delta}| < \xi$ .
- e) A penumbra terminator point is found when  $|\bar{\delta}| = \kappa$ .
- f) An umbra terminator point is found when  $|\bar{\delta}| = \xi$ .

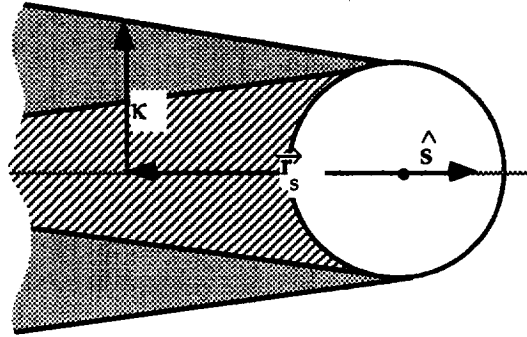


Figure 5. Location of the penumbral cone terminator at the projected spacecraft location.

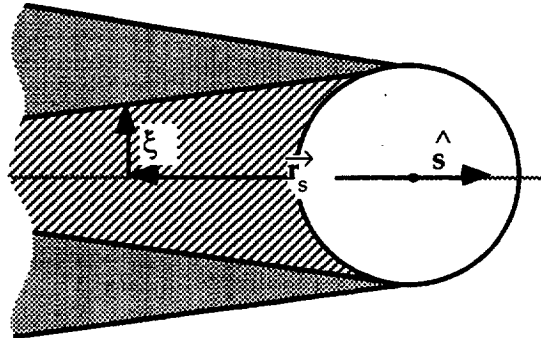


Figure 6. Location of the umbral cone terminator at the projected spacecraft location.

Since the methodology only deals with the magnitudes of the  $\bar{\delta}$  vector and the  $\kappa$  and  $\xi$  parameters, the determination of an entry or exit terminator point requires additional consideration. If the analysis is performed by advancing in eccentric anomaly<sup>11</sup> until the orbit is completed, then the following observations can be made:

- a) If at the beginning of the analysis  $|\bar{\delta}| > \kappa$  and  $|\bar{\delta}| > \xi$ , the spacecraft is initially in the sunlight. The first terminator encounter, if any, must be a penumbra entry

point. The second terminator encounter may be either an umbra entry or a penumbra exit. If a penumbra exit is found, the analysis for this orbit is completed. If an umbra entry point is found, the third encounter must be an umbra exit, followed by a penumbra exit. Then, the orbit analysis is completed.

If  $t_{pin}$  is the time of penumbra entry,  $t_{pex}$  is the time of penumbra exit,  $t_{uin}$  is the time of umbra entry, and finally  $t_{uex}$  is the umbra exit time, the time of shadow passage is determined as

$$\text{Time in umbra} = t_{uex} - t_{uin} \quad (9)$$

and

$$\text{Time in penumbra} = t_{pex} - t_{uex} + t_{uin} - t_{pin}. \quad (10)$$

- b) If at the beginning of the analysis  $|\bar{\delta}| < \kappa$  and  $|\bar{\delta}| < \xi$ , the spacecraft is initially in umbral shadow. The first terminator encounter must be an umbra exit point, followed by a penumbra exit. After a period of sunlight, the penumbra entry point is found, followed by the umbra entry. The finding of all terminator points completes the analysis of the orbit.

If  $t_{per}$  is the period of the orbit, the time of shadow passage can be calculated as

$$\text{Time in umbra} = t_{uex} + t_{per} - t_{uin} \quad (11)$$

and

$$\text{Time in penumbra} = t_{pex} - t_{uex} + t_{uin} - t_{pin}. \quad (12)$$

Since the initial problem time is only an offset, it does not appear in the time equations.

- c) If at the beginning of the analysis  $|\bar{\delta}| < \kappa$  and  $|\bar{\delta}| > \xi$ , the spacecraft is initially in the penumbral region. Then the first terminator encounter can either be an umbra entry or a penumbra exit. If the penumbra exit is found, the analysis is completed for the orbit. If instead, the umbra entry terminator is found, then it must be followed by umbra exit, penumbra exit, and finally by a penumbra entry.

The time of shadow passage can be determined from

$$\text{Time in umbra} = t_{uex} - t_{uin} \quad (13)$$

and

$$\text{Time in penumbra} = t_{\text{pex}} + t_{\text{per}} - t_{\text{pin}} - \text{Time in umbra} \quad (14)$$

Finally, the time in sunlight is simply calculated as the total orbit period less the time spent in shadow.

### Determination of the Spacecraft Location

The definition of the relationship that exists between two coordinate systems sharing a common origin is the basis for the calculation of the  $\vec{r}_{M50}$  vector. This definition may be obtained from any of three mathematical treatments: mainly the Euler angle, the direction cosine matrix, and the quaternion. Until the development of the digital computer, the Euler angle definition was widely used due to its geometrical simplicity and clear visualization.<sup>12</sup> The digital computation advancement of the mid-1960s marked the beginning of the use of the direction cosine matrix treatment since the computation methodologies were more suitable for computer programming, particularly when successive transformations of a body with respect to a fixed reference frame were defined. The use of the direction cosine matrix methodology is still common today. The third mathematical treatment is through definition of the quaternion.

### Quaternions

An infrequently used mathematical treatment of body transformations is the quaternion. This treatment was first devised by Sir William Rowan Hamilton<sup>13</sup> in 1843. This approach makes use of Euler's theorem which states that any real transformation of one coordinate system with respect to a fixed reference system (sharing a common origin) can be described through a single rotation called principal rotation about a single axis called principal axis.

A quaternion is a compact representation of a principal rotation about the principal axis and can be represented<sup>12-17</sup> as an ordered quadruple of real numbers

$$\begin{aligned} q_{AB} &= [q_1, q_2, q_3, q_4] \\ q_{AB} &= \left[ \cos \frac{f}{2}, e_x \sin \frac{f}{2}, e_y \sin \frac{f}{2}, e_z \sin \frac{f}{2} \right], \end{aligned} \quad (15)$$

or expressed in vector form<sup>13</sup> as an addition of a scalar and a vector

$$\begin{aligned} q_{AB} &= \text{scalar} + \text{vector} \\ q_{AB} &= q_1 + q_2 \hat{i} + q_3 \hat{j} + q_4 \hat{k}. \end{aligned} \quad (16)$$

The definition of the quaternion is subject to the normality condition

$$q_1^2 + q_2^2 + q_3^2 + q_4^2 = 1. \quad (17)$$

The treatment of quaternions is much like the direction cosine matrix in that a successive order of transformations results in a total transformation quaternion that is obtained through successive quaternion multiplication. The advantage of using quaternions results from the reduced computational load associated with the calculation of the total transformation quaternion. However, the computational load savings are only realized when a conversion of the total transformation quaternion to the equivalent total transformation matrix is not required and when the interchangeability property of the quaternion multiplication<sup>12</sup> is used whenever possible. As seen from the representation of the quaternion, the definition the quaternion requires four elements versus nine elements required to define a direction cosine matrix. Therefore, an added benefit is immediately realized from the reduced computer memory requirements and number of elements that need to be manipulated. It is therefore recognized that by using quaternion algebra, the calculation of transformations required for the determination of shadow passage are significantly improved. This allows for the use of an iterative process without severely impacting computation time.

### Quaternion Algebra

The advantages of quaternion manipulation for guidance and control were recognized early in the development of the Space Shuttle Orbiter. Several internal NASA publications<sup>15-17</sup> describing the Shuttle onboard software manipulation of quaternions were an important consideration in the development of the quaternion algebra defined in this section. Most importantly, the quaternion multiplication and the vector transformation through a quaternion will be described.

The vectorial definition of the quaternion allows for the development of quaternion algebra in the classical sense. If two quaternions, Q and P, are defined as

$$Q = (q_1, q_2, q_3, q_4) \quad (18)$$

$$P = (p_1, p_2, p_3, p_4)$$

then the fundamental definitions<sup>17</sup> are

a) Equality:  $Q=P$ , when and only when

$$q_1 = p_1, q_2 = p_2, q_3 = p_3, \text{ and } q_4 = p_4 \quad (19)$$

b) Addition:

$$Q + P = (q_1 + p_1, q_2 + p_2, q_3 + p_3, q_4 + p_4) \quad (20)$$

b) Subtraction:

$$Q - P = (q_1 - p_1, q_2 - p_2, q_3 - p_3, q_4 - p_4) \quad (21)$$

c) Multiplication by a scalar:

$$aQ = (aq_1, aq_2, aq_3, aq_4) \quad (22)$$

d) The quaternion product:

$$QP = (q_1 + q_2i + q_3j + q_4k)(p_1 + p_2i + p_3j + p_4k). \quad (23)$$

If we express the scalar part as  $S$  and the vector part as  $\vec{V}$ , the product may be written as

$$QP = (S_Q + \vec{V}_Q)(S_P + \vec{V}_P). \quad (24)$$

Manipulating this expression we obtain

$$QP = S_Q S_P + S_Q \vec{V}_P + \vec{V}_Q S_P + (\vec{V}_Q \times \vec{V}_P) - (\vec{V}_Q \bullet \vec{V}_P). \quad (25)$$

This expression has been shown in the literature<sup>12,13,17</sup> in matrix form as

$$QP = \begin{bmatrix} q_1 & -q_2 & -q_3 & -q_4 \\ q_2 & q_1 & q_4 & -q_3 \\ q_3 & -q_4 & q_1 & q_2 \\ q_4 & q_3 & -q_2 & q_1 \end{bmatrix} \begin{bmatrix} p_1 \\ p_2 \\ p_3 \\ p_4 \end{bmatrix}. \quad (26)$$

If the order of the quaternion is reversed such that

$$PQ = S_P S_Q + S_P \vec{V}_Q + \vec{V}_P S_Q + (\vec{V}_P \times \vec{V}_Q) - (\vec{V}_P \bullet \vec{V}_Q), \quad (27)$$

the resultant matrix form is

$$PQ = \begin{bmatrix} p_1 & -p_2 & -p_3 & -p_4 \\ p_2 & p_1 & -p_4 & p_3 \\ p_3 & p_4 & p_1 & -p_2 \\ p_4 & -p_3 & p_2 & p_1 \end{bmatrix} \begin{bmatrix} q_1 \\ q_2 \\ q_3 \\ q_4 \end{bmatrix}. \quad (28)$$



If the resultant matrix forms of equations 26 and 28 are simplified, both will give

$$\begin{aligned}
(QP)_1 &= (PQ)_1 = p_1q_1 - p_2q_2 - p_3q_3 - p_4q_4 \\
(QP)_2 &= (PQ)_2 = p_1q_2 + p_2q_1 + p_3q_4 - p_4q_3 \\
(QP)_3 &= (PQ)_3 = p_1q_3 - p_2q_4 + p_3q_1 + p_4q_2 \\
(QP)_4 &= (PQ)_4 = p_1q_4 + p_2q_3 - p_3q_2 + p_4q_1
\end{aligned} \tag{29}$$

showing the interchangeability of the quaternion multiplication.

The 4X4 matrices of equations 26 and 28 are defined<sup>12</sup> as the quaternion matrices. Notice that the only difference between quaternion matrices in equations 26 and 28 is the transmuted nature of the minor matrix of the first element. If we describe a transformation from the A reference frame to a B frame, and then from the B to the C frame, we can express the quaternion multiplication in a matrix form as

$$Q_{C \leftarrow A} = [M]_{C \leftarrow B} Q_{B \leftarrow A} \tag{30}$$

or

$$Q_{C \leftarrow A} = [M]_{B \leftarrow A}^t Q_{C \leftarrow B} \tag{31}$$

where  $[M]_{B \leftarrow A}^t$  is the transmuted quaternion matrix of the A->B transformation. If an additional transformation from C->D is imposed, then the total transformation can be expressed in matrix form as

$$Q_{D \leftarrow A} = [M]_{D \leftarrow C} [M]_{C \leftarrow B} Q_{B \leftarrow A} \tag{31}$$

or

$$Q_{D \leftarrow A} = [M]_{D \leftarrow C} [M]_{B \leftarrow A}^t Q_{C \leftarrow B} \tag{32}$$

and

$$Q_{D \leftarrow A} = [M]_{B \leftarrow A}^t [M]_{D \leftarrow C} Q_{C \leftarrow B} \tag{33}$$

In general

$$[M]_{B \leftarrow A}^t [M]_{D \leftarrow C} = [M]_{D \leftarrow C} [M]_{B \leftarrow A}^t \tag{34}$$

is a property that can be extended to the product of any number of quaternions.

## Vector Transformations

Given, without proof,<sup>15-18</sup> a vector is transformed from one coordinate system to another by

$$\bar{v}_D = Q_{D \leftarrow A} \bar{v}_A Q_{D \leftarrow A}^* \quad (35)$$

where  $Q_{D \leftarrow A}^*$  is the conjugate of  $Q_{D \leftarrow A}$ . The conjugate of a quaternion represented, for example, by equation 15 is defined<sup>15-18</sup> as

$$q_{AB} = [q_1, -q_2, -q_3, -q_4]. \quad (36)$$

The manipulation of equation 35 is through normal quaternion multiplication, where  $\bar{v}_A$  is treated as a quaternion with a zero scalar element.

## Motion in the Orbit Plane

The motion in the orbit plane, as shown in Figure 7, is obtained in part from the polar equation of the ellipse

$$r = \frac{a(1-e^2)}{1+e \cos v'} \quad (37)$$

which can also be expressed in terms of the eccentric anomaly<sup>11</sup> as

$$r = a(1 - e \cos E). \quad (38)$$

In Figure 7, the subscripts sc and p refer to the spacecraft and planet coordinate systems, respectively.

The relationship between the eccentric anomaly and the true anomaly<sup>11</sup> is given by

$$\tan \frac{1}{2} v' = \sqrt{\frac{1+e}{1-e}} \tan \frac{1}{2} E. \quad (39)$$

The time of flight is calculated from Kepler's equation<sup>11,14</sup>

$$M = E - e \sin E = \sqrt{\frac{\mu}{a^3}} (t - T), \quad (40)$$

where T is the time of passage through pericenter.

## Calculation of the $\bar{r}_{M50}$ Vector

As mentioned previously, the calculation of the  $\bar{r}_{M50}$  vector is performed in the M50 reference frame. The description of this vector is shown in Figure 8, as defined by the Keplerian elements.

Note that the orbit perturbation parameters are modeled as time variations in right ascension of the ascending node,  $\Omega$ , and argument of pericenter,  $\omega$ .

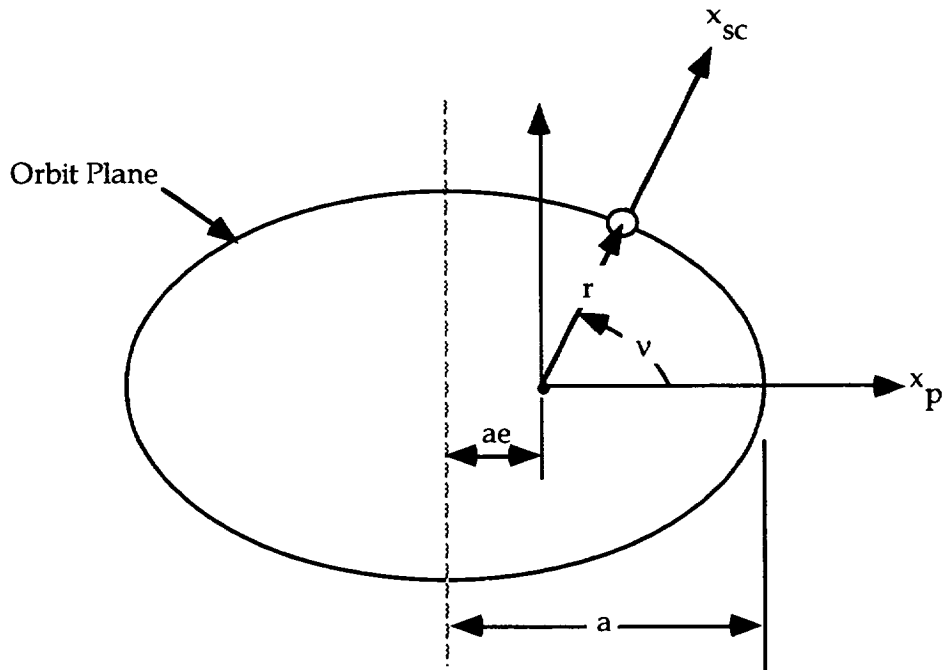


Figure 7. Polar coordinate definition of in-plane orbit parameters.

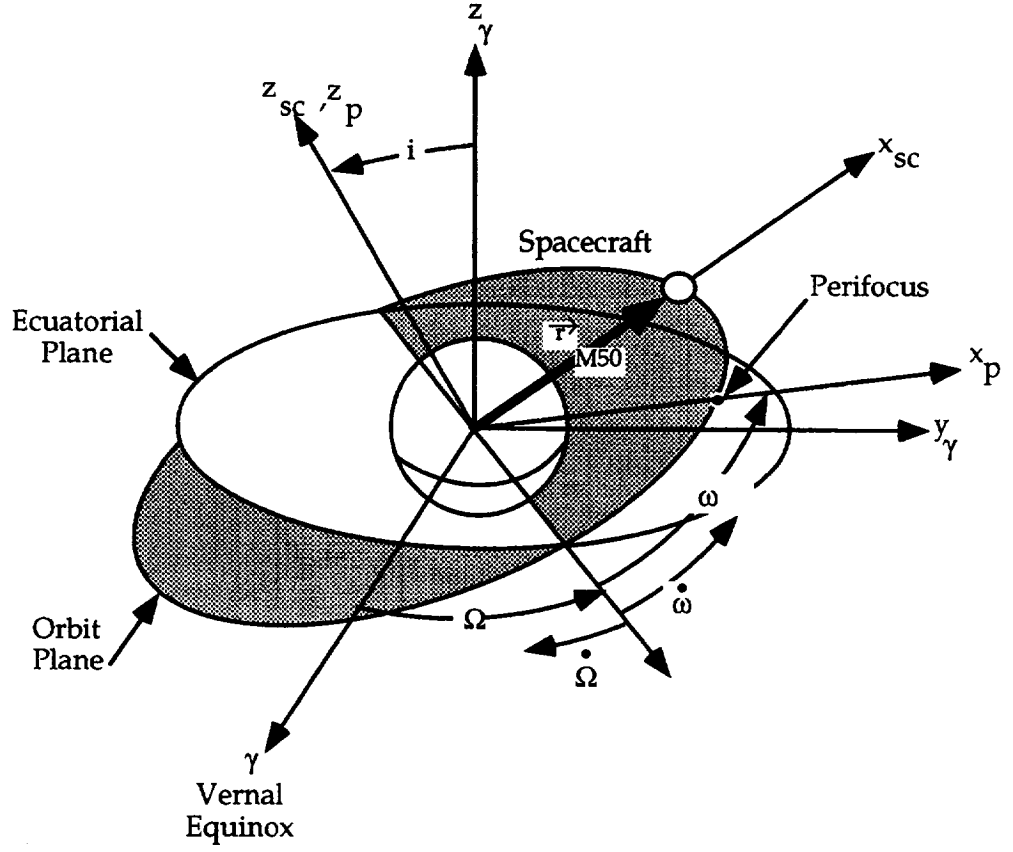


Figure 8. Definition of spacecraft location in the M50 reference frame.

The  $\vec{r}_{M50}$  vector is obtained from

$$\vec{r}_{M50} = r \cdot (\hat{r}_{p \rightarrow sp}), \quad (41)$$

where  $\hat{r}_{p \rightarrow sp}$  is the unit vector that points from the center of the planet to the spacecraft, and  $r$  is obtained from equation 37 or 38. The unit vector  $\hat{r}_{p \rightarrow sp}$  is obtained from a simple sequence of transformations, mainly

$$Q \vec{r}_{M50} = Q_{(\omega+\nu)} Q_i Q_\Omega \quad (42)$$

and

$$\vec{r}_{M50} = Q_{M50} \hat{r}_\gamma Q_{M50}^*, \quad (43)$$

where  $\hat{r}_\gamma$  is the reference vector  $\{1,0,0\}$ .

In equation 42, the rotation sequence is obtained by first, a z-axis rotation

$$Q_{\Omega} = [\cos \frac{\Omega}{2}, 0., 0., -\sin \frac{\Omega}{2}], \quad (44)$$

followed by an x-axis rotation

$$Q_i = [\cos \frac{i}{2}, -\sin \frac{i}{2}, 0., 0.], \quad (45)$$

and finally by another z-axis rotation, which by equation 20 can be represented as

$$Q_{(\omega+v)} = [\cos \frac{(\omega+v)}{2}, 0., 0., -\sin \frac{(\omega+v)}{2}]. \quad (46)$$

It should be noted by the reader that with little or no variation in right ascension of the ascending node and orbit inclination, the calculation  $Q_i Q_{\Omega}$  of equation 42 may be performed only once for each orbit analysis, thereby saving a significant amount of computational time.

In quaternion matrix form, equation 42 may also be expressed as

$$Q_{r_{M50}} = [M]_{(\omega+v)} [M]_i Q_{\Omega} \quad (47)$$

which by relations 32 and 33 can also be expressed as

$$Q_{r_{M50}} = [M]_{\Omega}^t [M]_i^t Q_{(\omega+v)}. \quad (48)$$

Once again, with little or no variation in  $\Omega$  and  $i$ , the matrix manipulation  $[M]_{\Omega}^t [M]_i^t$  may be performed only once per orbit analysis.

With the flexibility that quaternion algebra offers, the terminator calculation method employed here is well suited for considering the variation in  $\Omega$  and  $\omega$  due to the effect of the  $J_2$  oblateness perturbation. The variation of these two parameters will have the most pronounced effect on the calculation of the terminator entry and exit times. In such a case, the  $\Omega$  and  $\omega$  parameters are determined by the following expressions:

$$\Omega(t) = \Omega_0 + \dot{\Omega}t \quad (49)$$

and

$$\omega(t) = \omega_0 + \dot{\omega}t, \quad (50)$$

where  $\Omega_0$  is the initial right ascension of the ascending node, and  $\omega_0$  is the initial argument of pericenter. In equations 49 and 50,  $\dot{\Omega}$  and  $\dot{\omega}$  are obtained<sup>11</sup> from

$$\dot{\Omega} = -\frac{3}{2} J_2 \left( \frac{r_{eq}}{p} \right)^2 \sqrt{\frac{\mu}{a^3}} \cos(i) \quad (51)$$

and

$$\dot{\omega} = \frac{3}{4} J_2 \left( \frac{r_{eq}}{p} \right)^2 \sqrt{\frac{\mu}{a^3}} [5 \cos^2(i) - 1] \quad (52)$$

where  $r_{eq}$  is the equatorial radius of the planet/moon,  $p$  is the parameter or semi-latus rectum, and  $J_2$  is the oblateness perturbation coefficient.

### Iterative Methodology

As mentioned in previous sections, the calculation of the shadow terminator points is solved by an iterative procedure. The iterative method presented here, however, is well-suited to inclusion of the perturbations while the orbit progresses. Hence, no prior determination of whether or not the solar motion and the rates of  $\omega$  and  $\Omega$  significantly affect the terminator locations need be made. A standard bisection method, as described for example, by Cheney, et al.,<sup>19</sup> was adopted for this application. The bisection method proves to be the most effective calculation methodology, since the shadow terminator variables  $\Delta_p = (|\delta| - \kappa)$  and  $\Delta_u = (|\delta| - \xi)$  will have opposite signs in the time interval containing the terminator, and the shadow function described by the time variation of the shadow terminator variables is continuous.

The analysis of an orbit is performed by advancing in eccentric anomaly. An analysis interval  $[\Delta_a, \Delta_b]$ , represented by

$$\Delta_{\phi,a} = \Delta_{\phi,a}[E_a(t_a)] \quad (53)$$

and

$$\Delta_{\phi,b} = \Delta_{\phi,b}[E_b(t_b)], \quad (54)$$

( $\phi$  is either  $p$  or  $u$  for penumbra or umbra, and  $t_b > t_a$ ) will contain a terminator point if  $\Delta_{\phi,a} > 0$  and  $\Delta_{\phi,b} < 0$ . To find this terminator point, an intermediate analysis point is created as represented by

$$\Delta_{\phi,c} = \Delta_{\phi,c} [E_c(t_c)] \quad (55)$$

where

$$t_c = \frac{1}{2}(t_a + t_b). \quad (56)$$

Ideally, a shadow terminator point is found at time  $t_c$  (note that  $t_b > t_c > t_a$ ), if  $\Delta_{\phi,c} = 0$ . However, this is seldom the case. Instead, a sequence of time interval assessments must be performed according to the observation that if

$$\Delta_{\phi,a} \Delta_{\phi,c} < 0, \quad (57)$$

then the shadow terminator must be located between times  $t_a$  and  $t_c$ . Similarly, if

$$\Delta_{\phi,b} \Delta_{\phi,c} < 0 \quad (58)$$

the shadow terminator is then in the time interval  $[t_c, t_b]$ . A new interval assessment is performed by selecting the time interval containing the shadow terminator. This sequence is repeated until  $\Delta_{\phi,c} - \Delta_{\phi,a} < \text{error}$  or  $\Delta_{\phi,b} - \Delta_{\phi,c} < \text{error}$ , where the error is a satisfactorily small number.

## Sample Cases

The mathematical methodology described in the previous sections was coded in standard FORTRAN in support of the development of the Thermal Constraint Attitude Design System (TCADS) analysis package. TCADS will help in the design of a spacecraft mission attitude timeline based on the definition of thermal and power constraints.

Five examples were chosen based on simulations that would exercise the capabilities of the methodology to the full extent. All simulations were performed with orbits about Earth. However, the method is applicable to any celestial body for which the necessary parameters are known. Physical constants used in these analyses were obtained from the Jet Propulsion Laboratory.<sup>20</sup> The examples are named as follows and covered individually in the following sections:

- High Inclination, Low-Earth Circular Orbit
- Sun Synchronous Orbit
- High Inclination Elliptical Orbit
- Geostationary Orbit
- Combined Released and Radiation Effects Satellite (CRRES)<sup>10</sup> Case Comparison
- Illustration of Conical versus Cylindrical Shadow Assumption

In the first five examples, the shadow terminator analysis was performed for 2 Earth years. The results are presented in plots of beta angle,  $\beta$ , variation versus time, and variation in percentage of orbit period spent in umbral and penumbral shadow as a function of time. The last example provides an assessment of time spent in Earth's shadow for both the cylindrical assumption<sup>5</sup> and the conical assumption using the current methodology.

The beta angle,  $\beta$ , is the angle between solar vector,  $\hat{s}$ , and its projection onto the orbit plane, and it is used in this analysis since it provides the thermal engineer a means of assessing the thermal environment experienced by an orbiting spacecraft.  $\beta$  is given by

$$\beta = \sin^{-1}(\hat{o} \bullet \hat{s}), \quad (59)$$

where  $\hat{o}$  is the orbit normal vector and  $\hat{s}$  is the unit solar vector. These unit vectors may be expressed by

$$\hat{s} = \begin{Bmatrix} \cos(\Gamma) \\ \sin(\Gamma) \cos(\epsilon) \\ \sin(\Gamma) \sin(\epsilon) \end{Bmatrix} \quad (60)$$

and

$$\hat{o} = \begin{Bmatrix} \sin(\Omega) \\ -\cos(\Omega) \sin(i) \\ \cos(i) \end{Bmatrix}, \quad (61)$$

where  $\Gamma$  is the ecliptic solar longitude and  $\epsilon$  is the obliquity of the ecliptic. As a planet moves about the sun,  $\Gamma$  will vary from 0 to  $2\pi$ . Additionally, the perturbation in  $\Omega$ , discussed earlier, will cause the vector  $\hat{o}$  to cone about the polar axis of the planet. The combined effect of these two variations gives rise to the change in  $\beta$  angle.

### High Inclination, Low-Earth Orbit

This example illustrates a typical high inclination, low altitude Earth orbit. In this case, the analysis begins the first day of spring 1994. The complete list of orbital parameters used to initialize the problem are listed in Table 1.



**Table 1. Orbital Parameters of Sample Case 1**

Semimajor Axis	6785.58 km
Eccentricity	0.0
Inclination	51.6°
Arg. of Pericenter	Undefined
Apsidal Rotation Rate	3.7326°/day
Initial Right Ascension	358.77°
Ascending Node Rate	-4.99°/day
Initial Solar Right Ascension	0.5866°
Initial Solar Declination	0.2400°

This case was selected to test the code over a beta angle range which would provide for the full range of shadowing situations. The orbit inclination and altitude selected provide for numerous precession cycles throughout the year as well as a number of periods of 100% sunlit orbits.

The results of this case are shown in Figures 9 and 10 for the beta angle variation and time spent in shadow as a function of time.

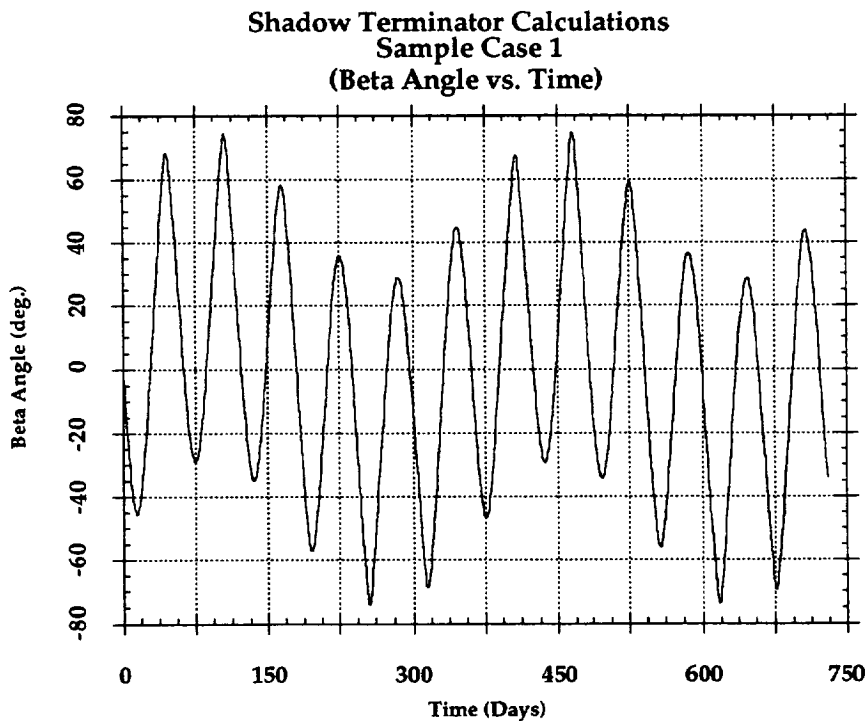


**Figure 9. Case 1: Beta angle variation with time.**

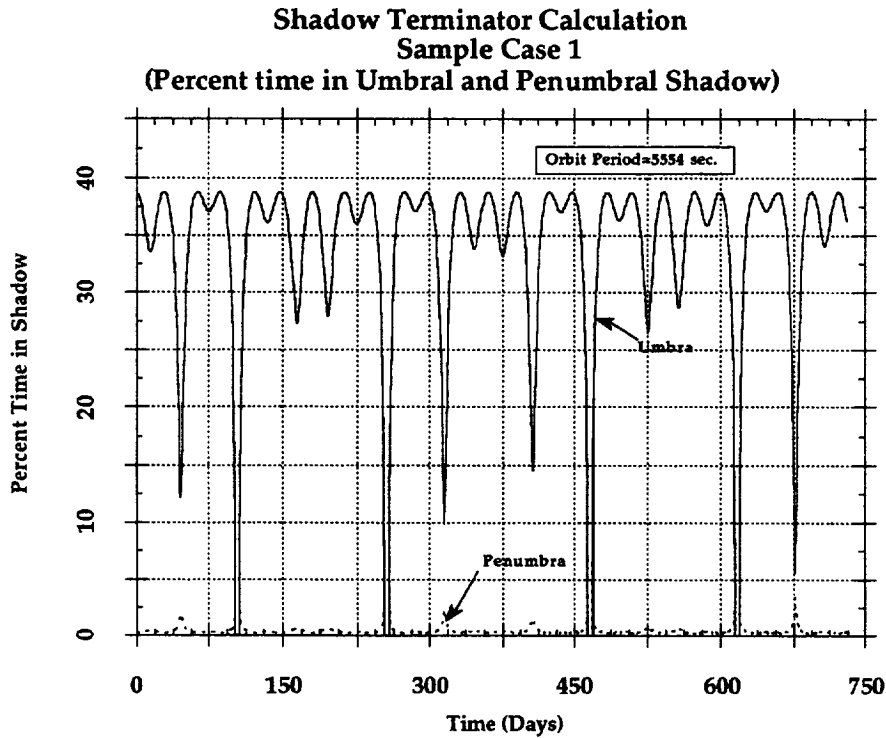


**Figure 10. Case 1: Percent time in shadow.**

### Sun-Synchronous Orbit

A typical sun-synchronous orbit is modeled in this example. Sun-synchronous orbits are useful for mapping spacecraft since they are flown at nearly a constant beta angle. This provides a consistent lighting environment for the sunlit side of the orbit. This is accomplished through use of a retrograde (i.e.,  $i > 90^\circ$ ) orbit which causes the ascending node to precess eastward. The altitude and inclination are selected such that the rate of movement of the ascending node closely matches the mean motion of the sun as it moves about the celestial sphere. A sun-synchronous orbit then should have a relatively flat beta angle versus time profile and an even flatter shadow time profile (since umbral shadow time variation is not extreme for a large range of beta angles about  $\beta=0^\circ$ ). This example also tests the retrograde motion capability of the algorithm.

The orbital parameters are presented in Table 2. The initial orbital parameters also correspond to the first day of spring 1994. The beta angle and shadow profiles are presented in Figures 11 and 12, respectively.

**Table 2. Orbital Parameters of Sample Case 2**

Semimajor Axis	7083.14 km
Eccentricity	0.0
Inclination	98.2°
Arg. of Pericenter	Undefined
Apsidal Rotation Rate	-3.105°/day
Initial Right Ascension	358.77°
Ascending Node Rate	0.9859°/day
Initial Solar Right Ascension	0.5866°
Initial Solar Declination	0.2400°

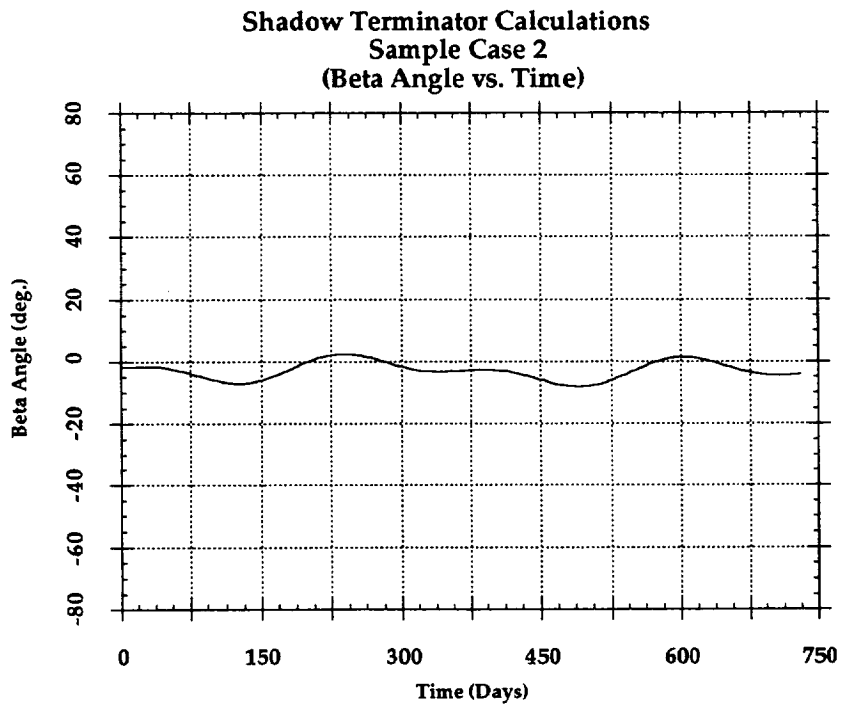


**Figure 11. Case 2: Beta angle variation versus time.**

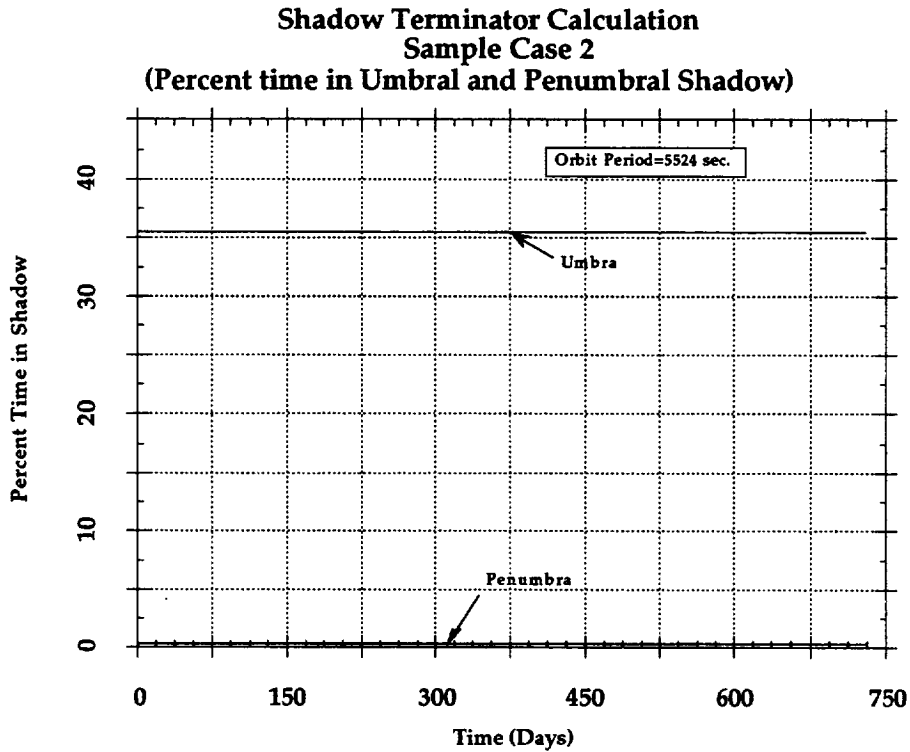


**Figure 12. Case 2: Percent time in shadow.**

### High Inclination Elliptical Orbit

Sample case 3 tests the algorithm on a high inclination elliptical orbit. The inclination selected causes the apsidal rotation rate to go to zero. The benefits of this orbit inclination are exploited by the Molniya spacecraft which maintains the apogee and perigee at desired locations to facilitate communications. The elliptic nature of the orbit tests the robustness of the algorithm over a variety of conditions. Since the precession of the ascending node is slow (compared to a low altitude orbit) fewer cycles of beta are seen.

The orbital parameters, corresponding to the first day of spring 1994, are presented in Table 3. The beta angle and shadow profiles are presented in Figures 13 and 14, respectively.

**Table 3. Orbital Parameters of Sample Case 3**

Semimajor Axis	42238.84 km
Eccentricity	0.8273
Inclination	63.3°
Initial Arg. of Pericenter	-63.3°
Apsidal Rotation Rate	0.00°/day
Initial Right Ascension	358.77°
Ascending Node Rate	-0.0599°/day
Initial Solar Right Ascension	0.5866°
Initial Solar Declination	0.2400°

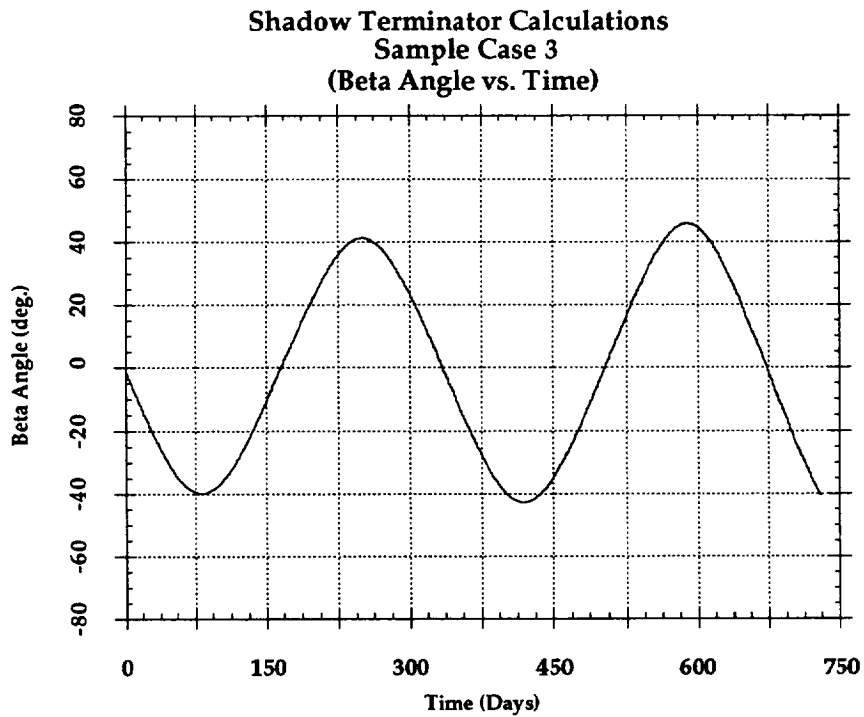


**Figure 13. Case 3: Beta angle variation versus time.**

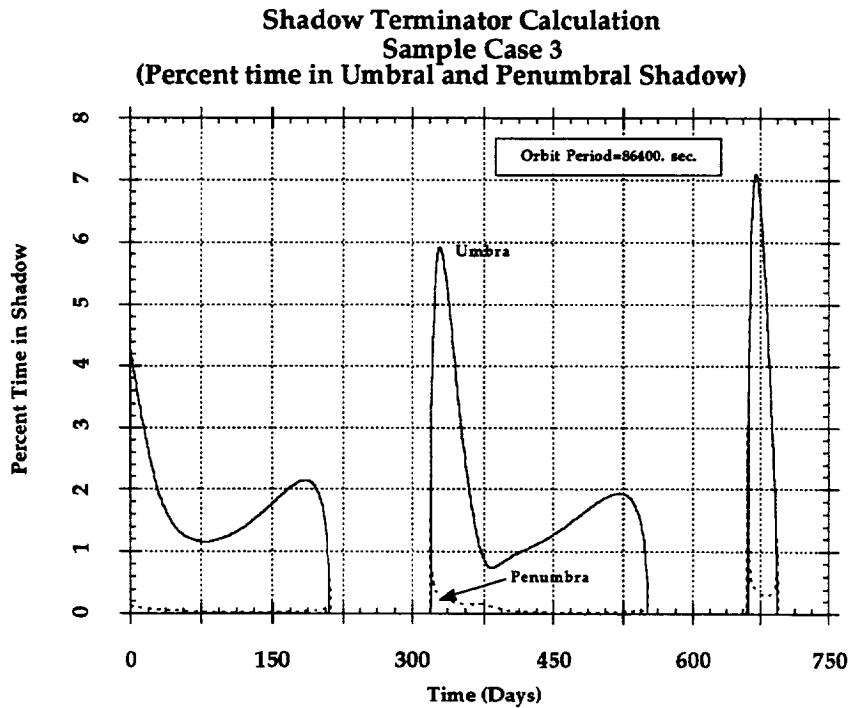


**Figure 14. Case 3: Percent time in shadow.**

### Geostationary Orbit

A geostationary orbit is modeled in this sample case. The altitude is selected such that the orbit period matches the rotation rate of the planet. This has the effect of keeping the spacecraft over a given point on the planet.

The orbital parameters are presented in Table 4. The beta angle and shadow profiles are presented in Figures 15 and 16, respectively.

**Table 4. Orbital Parameters of Sample Case 4**

Semimajor Axis	42305.08 km
Eccentricity	0.00
Inclination	0.00°
Arg. of Pericenter	Undefined
Apsidal Rotation Rate	0.027°/day
Initial Right Ascension	219.77°
Ascending Node Rate	-0.0133°/day
Initial Solar Right Ascension	0.5866°
Initial Solar Declination	0.2400°

**Shadow Terminator Calculations  
Sample Case 4  
(Beta Angle vs. Time)**

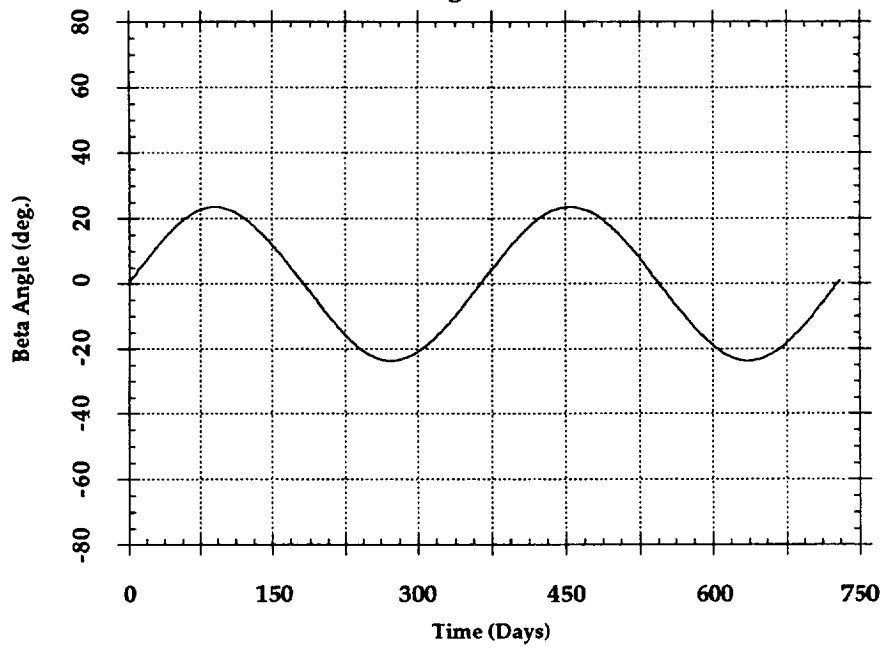


**Figure 15. Case 4: Beta angle variation versus time.**

**Shadow Terminator Calculation  
Sample Case 4  
(Percent time in Umbral and Penumbral Shadow)**

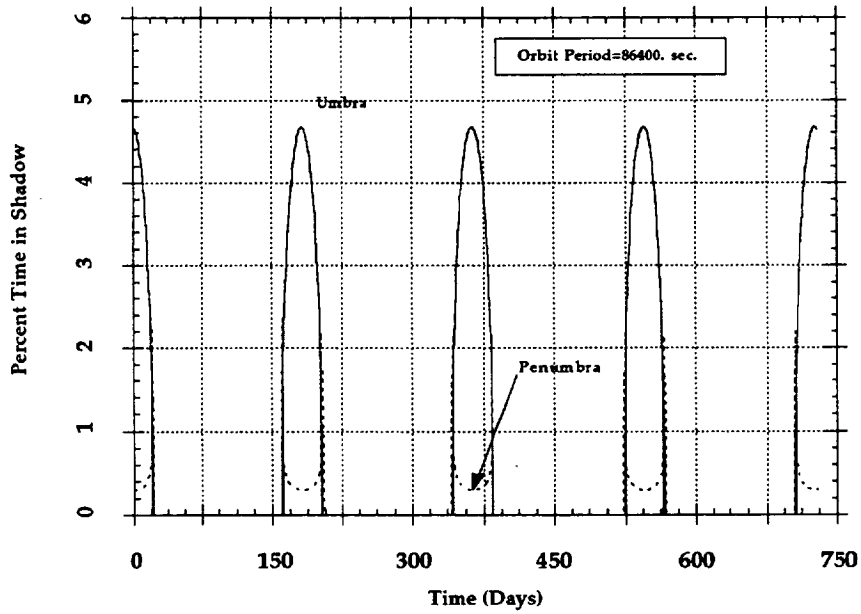


**Figure 16. Case 4: Percent time in shadow.**

## CRRES Orbit

This sample case was selected as a cross-check of the TCADS software, with the sample case presented in Mullins.<sup>10</sup> Mullins describes a method for solving the terminator problem through solution of a quartic polynomial. The shadow profile curve was successfully re-created using the algorithm. The beta angle profile was also checked against results from the Thermal Synthesizer System software.<sup>5</sup>

The orbital parameters are presented in Table 5. The beta angle and shadow profiles are presented in Figures 17 and 18, respectively. In this particular case, the Mullins assumption of constant parameters (i.e., variation parameters described by equations 49 and 50 are only updated at the beginning of an analysis orbit and held constant for the orbit) appears to be a valid assumption, since no significant differences in calculated percent time in shade are observed.

**Table 5. Orbital Parameters of Sample Case 5**

Semimajor Axis	24450 km
Eccentricity	0.725
Inclination	18.0°
Initial Arg. of Pericenter	180°
Apsidal Rotation Rate	0.7064°/day
Initial Right Ascension	68°
Ascending Node Rate	-0.3812°/day
Initial Solar Right Ascension	83.041°
Initial Solar Declination	23.27°



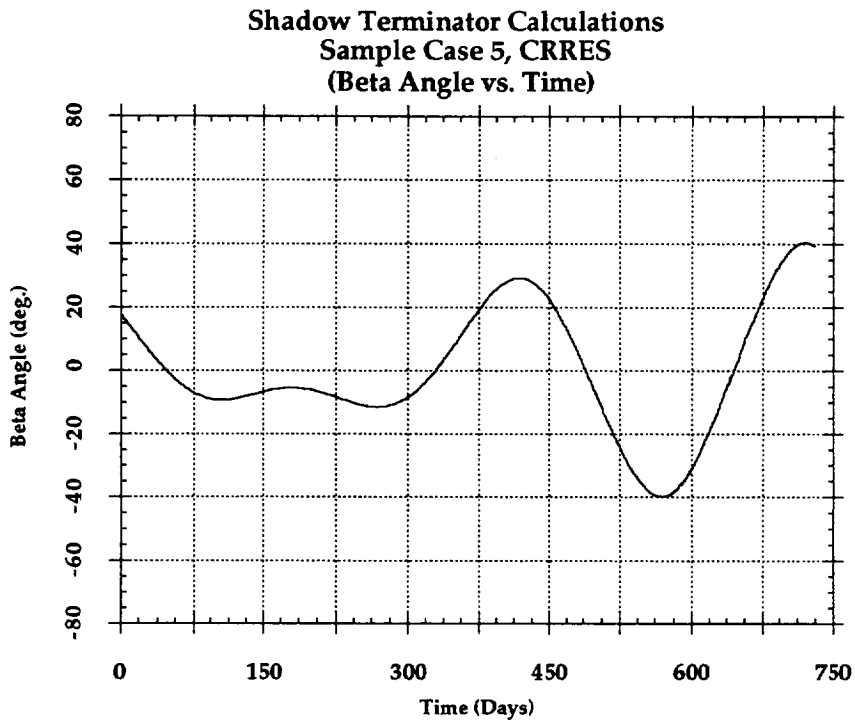


Figure 17. Case 5: Beta angle variation versus time.

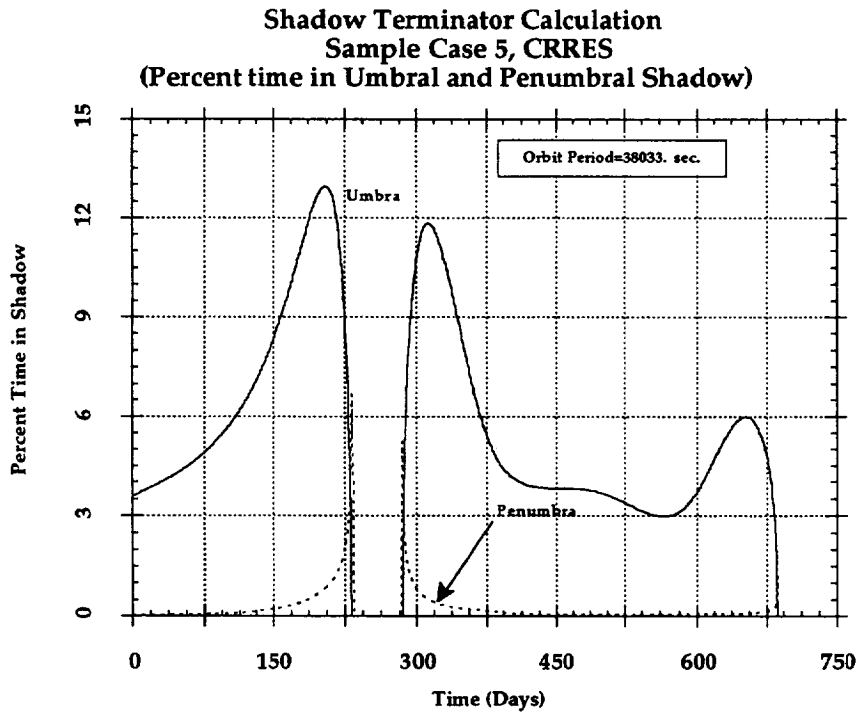


Figure 18. Case 5: Percent time in shadow.

## Conical versus Cylindrical Assumption

This test case was created as an illustration of the potential for error of using a cylindrical shadow assumption. An elliptical orbit was specified using the Thermal Synthesizer System software<sup>5</sup> such that its path would barely skim the cylindrical umbral shadow. Next, the same orbit was modeled using the TCADS algorithm. The orbit parameters used are given in Table 6.

**Table 6. Orbital Parameters of Sample Case 6**

Semimajor Axis	44859.14 km
Eccentricity	0.8408
Inclination	4.47°
Initial Arg. of Pericenter	90°
Apsidal Rotation Rate	0.2496°/day
Initial Right Ascension	-90°
Ascending Node Rate	-0.1254°/day
Initial Solar Right Ascension	0.131°
Initial Solar Declination	0.054°

The cylindrical assumption applied to the parameters presented above produced an umbral shadow time of 0.955% (~15 min.)(using the Thermal Synthesizer System software). A cylindrical shadow assumption does not provide for any penumbral shadow. When calculated using the routine created for TCADS, it was determined that the spacecraft would spend 0% of the orbit in the umbral shadow and 7.60% of the orbit period in the penumbral shadow: almost 2 hours in less than full sunlight conditions. The implication of this is that quickly reacting spacecraft components will be affected by this reduction in solar flux. Hence, a more accurate characterization of the umbral and penumbral shadows will lead to a more accurate thermal analysis with fewer required simplifying assumptions. A comparison of the cylindrical versus conical assumption is given in Table 7.

**Table 7. Comparison of Conical and Cylindrical Shadow Assumptions**

Component	Conical Assumption (Minutes)	Cylindrical Assumption (Minutes)
Umbra	0.0	15.1
Penumbra	119.8	Not calculated

## References

1. Stoddard, L.G., "Eclipse of an Artificial Earth Satellite," *Astronaut. Sci. Rev.*, III, 9-16, 1961.
2. Cunningham, F.G., "Calculation of the Eclipse Factor for Elliptical Satellite Orbits," NASA TN D-1347, 1962.
3. Pierce, D., "A Rapid Method for Determining the Percentage of a Circular Orbit in the Shadow of the Earth," *Astronaut. Sci. Rev.*, IX, 89-92, 1962.
4. Long, A.C., Cappellari, J.O., Velez, C.E., and Fuchs, A.J., "Goddard Trajectory Determination System (GTDS) Mathematical Theory, Revision 1," NASA/GSFC N911-70514, 1989.
5. Lockheed Missiles and Space Company "Thermal Synthesizer System, Theory Manual," LMSC/F191409, Sunnyvale, California, 1992.
6. Peckman, G.W., "The Orbital Shadow Times of an Earth Satellite," Institute of Technology, Air Univ., U.S. Air Force, GAE/AE-60-09, 1960.
7. Fixler, S.Z., "Umbra and Penumbra Eclipse Factors for Satellite Orbits," *AIAA Journal*, 2 [8], 1455-1457, 1964.
8. Dreher, P.E., "Satellite Shadow Times," NASA TM X-53389, 1965.
9. Taff, L.G., *Celestial Mechanics, A Computational Guide for the Practitioner*, John Wiley and Sons, New York, 1985.
10. Mullins, L.D., "Calculating Satellite Umbra/Penumbra Entry and Exit Positions and Times," *The Journal of Astronautical Sciences*, 39 [4], 411-422, 1991.
11. Battin, R.H., *An Introduction to the Mathematics and Methods of Astrodynamics*, AIAA Education Series edited by J.S. Przemieniecki, 1987.
12. Ickes, B.P., "A New Method for Performing Digital Control System Attitude Computations Using Quaternions," *AIAA Journal*, 8 [1], 13-17, 1970.
13. Hamilton, Sir William Rowan, *Elements of Quaternions*, Chelsea Publishing Company, New York, N.Y., 1969.
14. Bate, R.R., Mueller, D.D., and White, J.E., *Fundamentals of Astrodynamics*, Dover Publications, Inc., New York, 1971.
15. Henderson, D.M., "Euler Angles, Quaternions, and Transformation Matrices," NASA JSC Report 12960, 1977.
16. Perry, E.L., "Quaternions and Their Use," NASA JSC Report 18652, 1982.
17. Sunkel, J.W. and Peters, W.H., "Quaternions for Control of the Space Shuttle," NASA JSC Report 11150, 1976.
18. Grubin, C., "Derivation of the Quaternion Scheme via the Euler Axis and Angle," *AIAA Journal*, 7 [10], 1261- 1263, 1970.
19. Cheney, W. and Kincaid, D., *Numerical Mathematics and Computing*, Brooks/Cole Publishing Company, Monterey, California, 1980.
20. Stetson, D., Jet Propulsion Laboratory, personal communications, 1991.

# REPORT DOCUMENTATION PAGE

Form Approved  
OMB No. 0704-0188

Public reporting burden for this collection of information is estimated to average 1 hour per response, including the time for reviewing instructions, searching existing data sources, gathering and maintaining the data needed, and completing and reviewing the collection of information. Send comments regarding this burden estimate or any other aspect of this collection of information, including suggestions for reducing this burden, to Washington Headquarters Services, Directorate for Information Operations and Reports, 1215 Jefferson Davis Highway, Suite 1204, Arlington, VA 22202-4302, and to the Office of Management and Budget, Paperwork Reduction Project (0704-0188), Washington, DC 20503.

1. AGENCY USE ONLY (Leave Blank)		2. REPORT DATE <p style="text-align: center;">April 1995</p>	3. REPORT TYPE AND DATES COVERED <p style="text-align: center;">NASA Technical Paper</p>	
4. TITLE AND SUBTITLE <p style="text-align: center;">Method for the Calculation of Spacecraft Umbra and Penumbra Shadow Terminator Points</p>			5. FUNDING NUMBERS	
6. AUTHOR(S) <p style="text-align: center;">Carlos R. Ortiz Longo and Steven L. Rickman</p>				
7. PERFORMING ORGANIZATION NAME(S) AND ADDRESS(ES) <p style="text-align: center;">Lyndon B. Johnson Space Center Structures and Mechanics Division Houston, Texas 77058</p>			8. PERFORMING ORGANIZATION REPORT NUMBERS <p style="text-align: center;">S-800</p>	
9. SPONSORING/MONITORING AGENCY NAME(S) AND ADDRESS(ES) <p style="text-align: center;">National Aeronautics and Space Administration Washington, DC 20546-0001</p>			10. SPONSORING/MONITORING AGENCY REPORT NUMBER <p style="text-align: center;">TP-3547</p>	
11. SUPPLEMENTARY NOTES				
12a. DISTRIBUTION/AVAILABILITY STATEMENT Unclassified/Unlimited Available from the NASA Center for AeroSpace Information (CASI) 800 Elkridge Landing Road Linthicum Heights, MD 21090-2934 (301) 621-0390			12b. DISTRIBUTION CODE	
13. ABSTRACT ( <i>Maximum 200 words</i> )  A method for calculating orbital shadow terminator points is presented. The current method employs the use of an iterative process which is used for an accurate determination of shadow points. This calculation methodology is required, since orbital perturbation effects can introduce large errors when a spacecraft orbits a planet in a high altitude and/or highly elliptical orbit. To compensate for the required iteration methodology, all reference frame change definitions and calculations are performed with quaternions. Quaternion algebra significantly reduces the computational time required for the accurate determination of shadow terminator points.				
14. SUBJECT TERMS <p style="text-align: center;">umbras, quaternions, iteration methodology/process, terminator lines</p>			15. NUMBER OF PAGES <p style="text-align: center;">35</p>	
			16. PRICE CODE	
17. SECURITY CLASSIFICATION OF REPORT <p style="text-align: center;">Unclassified</p>	18. SECURITY CLASSIFICATION OF THIS PAGE <p style="text-align: center;">Unclassified</p>	19. SECURITY CLASSIFICATION OF ABSTRACT <p style="text-align: center;">Unclassified</p>	20. LIMITATION OF ABSTRACT <p style="text-align: center;">Unlimited</p>	